Interaction between carotid baroregulation and the pulsating heart: a mathematical model

MAURO URSINO
Department of Electronics, Computer Science and Systems, University of Bologna, I40136 Bologna, Italy

Ursino, Mauro. Interaction between carotid baroregulation and the pulsating heart: a mathematical model. *Am. J. Physiol.* 275 (*Heart Circ. Physiol.* 44): H1733–H1747, 1998.—A mathematical model of short-term arterial pressure control by the carotid baroreceptors in pulsatile conditions is presented. The model includes an elastance variable description of the left and right heart, the systemic (splanchnic and extrasplanchnic) and pulmonary circulations, the afferent carotid baroreceptor pathway, the sympathetic and vagal efferent activities, and the action of several effector mechanisms. The latter mechanisms work, in response to sympathetic and vagal action, by modifying systemic peripheral resistances, systemic venous unstressed volumes, heart period, and end-systolic elastances. The model is used to simulate the interaction among the carotid baroreflex, the pulsating heart, and the effector responses in different experiments. In all cases, there has been satisfactory agreement between model and experimental results. Experimental data on heart rate control can be explained fairly well by assuming that the sympathetic-parasympathetic systems interact linearly on the heart period. The carotid baroreflex can significantly modulate the cardiac function curve. However, this effect is masked in vivo by changes in arterial and atrial pressures. During heart pacing, cardiac output increases with frequency at moderate levels of heart rate and then fails to increase further because of a reduction in stroke volume. Shifting from nonpulsatile to pulsatile perfusion of the carotid sinuses decreases the overall baroreflex gain and significantly modifies operation of the carotid baroreflex. Finally, a sensitivity analysis suggests that venous unstressed volume control plays the major role in the early hemodynamic response to acute hemorrhage, whereas systemic resistance and heart rate controls are a little less important.

baroreflex; cardiac elastance; unstressed volume; atrial pacing

SHORT-TERM SYSTEMIC arterial pressure control in humans and mammals is carried out by a sophisticated multi-input, multi-feedback system termed the baroreflex. The complex structure of the baroreflex, its function, and the role played by the different mechanisms have been the subject of a multitude of experimental studies in the past decades (for review, see Refs. 13 and 37). These studies provide quite a complete description of the different components in both dynamic and static conditions. Nevertheless, understanding the behavior of the baroreflex system as a whole is still a hard problem, which is yet to be completely resolved. The main difficulties derive from the fact that the interactions among the components are strongly nonlinear in nature; hence, the overall system response may be largely different from the sum of the individual actions.

Mathematical modeling based on nonlinear system theory may help our understanding of the cardiovascular system. Indeed, several such models of the baroreflex have been proposed in past years (3, 17, 35). In a recent paper (47), Ursino et al. presented a model of short-term carotid baroregulation that emphasizes the role of active changes in venous capacity in maintaining cardiac output during volume perturbations.

Despite the existence of these models, many aspects of short-term arterial pressure control are yet to be modeled accurately. First, arterial pressure pulsatility has a considerable effect on the carotid baroreflex. Shifting from nonpulsatile to pulsatile perfusion of the carotid sinuses modifies the frequency in the sinus nerve (6) and alters baroreflex gain (1, 39). Second, the carotid baroreflex can significantly modify the flow-generating capacity of the heart, i.e., the Starling relationship (15, 22). This effect is evidenced by experiments performed at constant systemic arterial pressure but in normal conditions is masked by simultaneous changes in preload and afterload. Third, the splanchnic and extrasplanchnic circulations have different roles in the baroreflex control, causing volume redistribution in response to hemodynamic perturbations (4).

The aim of this paper is to present the main aspects of a new mathematical model of the baroreflex devoted to the analysis of these problems. In particular, much attention is focused on modeling the pulsating heart and on its interaction with the carotid baroreflex control system. Even though several models of the heart as a pulsating pump have been formulated in past years, I am not aware of any computer study that elucidates the strict interaction among the pumping heart, pressure pulsatility, and carotid baroreflex.

Simulations concern a time period of only 1–2 min after hemodynamic perturbations. During this period, in fact, fluid shift across the capillary wall and hormonal regulation have negligible effects on the regulatory response.

The present article is structured as follows. First, a qualitative description of the model is presented and parameter values are assigned. Subsequently, the model is validated by simulating experimental results concerning the interaction among the heart, pressure pulsatility, and the carotid baroreflex in open-loop conditions. Finally, the system is simulated in closed-loop conditions, to clarify the relative role of each mechanism in the response to hemorrhage.

The costs of publication of this article were defrayed in part by the payment of page charges. The article must therefore be hereby marked "*advertisement*" in accordance with 18 U.S.C. Section 1734 solely to indicate this fact.

0363-6135/98 $5.00 Copyright © 1998 the American Physiological Society

Downloaded from http://ajpheart.physiology.org/ by 10.220.33.2 on September 9, 2017

QUALITATIVE MODEL DESCRIPTION

The present model constitutes a generalization of the mathematical model described in a previous paper (47). The main improvements and new aspects are as follows. *1*) The heart is described as a pulsatile pump. To this end, the activity of the ventricles is simulated by an elastance variable model (38). *2*) Because arterial pressure is pulsatile in nature, a more accurate description of the aortic and pulmonary input impedances is required, valuable also in the midfrequency range. For this reason, the new model discriminates between large arterial vessels and peripheral arterioles and includes inertial terms in arteries. *3*) The rate-dependent component of the carotid baroreceptors is included, because it plays a major role in the pulsatile regime. A distinction is made between the afferent portion of the carotid baroreflex, the efferent sympathetic and vagal pathways, and the effector responses. *4*) Reflex heart contractility control, which was only implicit in the previous model, is explicitly considered in the present model. *5*) Heart rate is controlled by both the sympathetic and the vagal activity. *6*) The systemic vascular bed is subdivided into the parallel arrangement of the splanchnic and extrasplanchnic circulations, which exhibit a different baroreflex response.

I describe here the main aspects of the heart, the vasculature, and the carotid baroreflex separately in qualitative terms. All equations can be found in the APPENDIX.

Vascular Compartments

The vascular system includes eight compartments, as shown in the hydraulic analog of Fig. 1. Five of these compartments are used to reproduce the systemic circulation, differentiating among the systemic arteries (subscript sa), the splanchnic peripheral and venous circulations (subscripts sp and sv, respectively), and the extrasplanchnic peripheral and venous circulations (subscripts ep and ev, respectively). Similarly, the other three compartments mimic the arterial, peripheral and venous pulmonary circulations (subscripts pa, pp, and pv, respectively). Subscripts la, lv, ra, and rv indicate the left atrium, left ventricle, right atrium, and right ventricle, respectively. Each compartment includes a hydraulic resistance (R_j), which accounts for pressure energy losses in the *j*th compartment, a compliance (C_j), which describes the amount of stressed blood volume stored at a given pressure, and an unstressed volume ($V_{u,j}$). For the sake of simplicity, the inertial effects of blood have been included only in the large artery compartments, in which blood acceleration is significant.

Equations relating pressure and flow in all points of the vascular system have been written by enforcing preservation of mass at the capacities in Fig. 1 and equilibrium of forces at the inertances (L_j) and by assuming that the total amount of blood initially contained in the vascular system is 5,300 ml.

The Heart as a Pump

The models for the right and the left heart are similar, with different values of parameters. The atrium is described as a linear capacity characterized by constant values of compliance and unstressed volume, i.e., the contractile activity of the atrium is neglected. Blood passes from the atrium to the ventricle through the atrioventricular valve, mimicked as the series arrangement of an ideal unidirectional valve in series with a constant resistance.

The contractile activity of the ventricle is described by means of a Voigt viscoelastic model, i.e., the series arrangement of a time-varying elastance, which accounts for the isometric pressure/volume function, and a time-varying resistance. This resistance mainly reflects the viscosity of the ventricle and increases with the contractile activity of muscle fibers (44). The elastance varies during the cardiac cycle as a consequence of the contractile activity of the ventricle. At diastole, when the muscle fibers are relaxed, the ventricle fills through an exponential pressure/volume function (Fig. 2, *top*), which reflects the elasticity both of the relaxed muscle and of its external constraints (mainly the pericardium). In contrast, in accordance with the work of Sagawa et al. (38), I adopted a linear pressure/volume function at end systole whose slope (usually called the end-systolic elastance) is denoted by E_{max}. Shifting from the end-diastolic to the end-systolic relationship is governed by a pulsating activation function $\varphi(t)$, with period T equal to the heart period. In this work, I used a sine square expression for $\varphi(t)$, as proposed by Piene (31). Moreover, heart period varies as a consequence of the baroreflex control action (see *Carotid Baroreflex*) whereas, according to data reported in Weissler et al. (49), I assumed that the duration of systole decreases linearly with the heart rate. Finally, blood flow leaving the ventricle depends on the aortic valve opening and on the difference between the isometric ventricle pressure and arterial pressure (afterload). The simulated time patterns of some hemodynamic quantities (systemic arterial pressure, left ventricle pressure, cardiac output) are shown in the middle and bottom panels of Fig. 2.

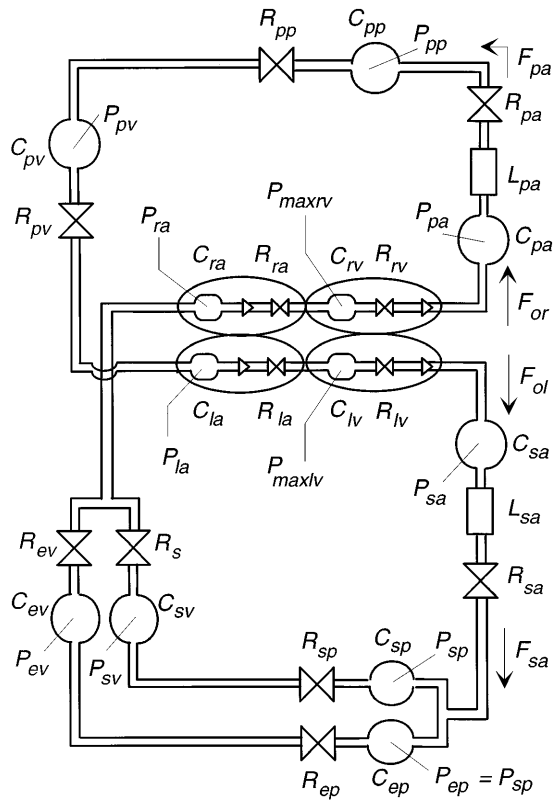

Fig. 1. Hydraulic analog of cardiovascular system. P, pressures; *R*, hydraulic resistances; C, compliances; *L*, inertances; F, flows; sa, systemic arteries; sp, splanchnic peripheral circulation, sv, splanchnic venous circulation; ep, extrasplanchnic peripheral circulation, ev, extrasplanchnic venous circulation; ra, right atrium; rv, right ventricle; pa, pulmonary arteries; pp, pulmonary peripheral circulation; pv, pulmonary veins; la, left atrium; lv, left ventricle; ol and or, output from left and right ventricle, respectively; $P_{max,rv}$ and $P_{max,lv}$, ventricle pressures in isometric conditions.

Downloaded from http://ajpheart.physiology.org/ by 10.220.33.2 on September 9, 2017

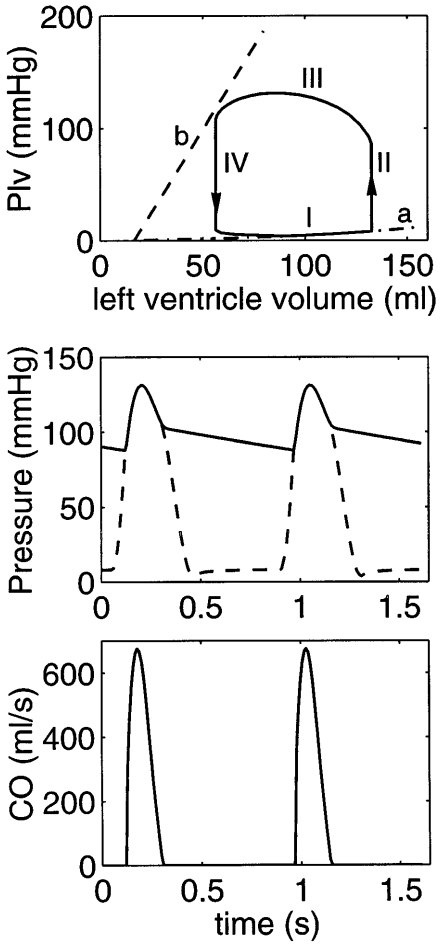

Fig. 2. Example of left ventricle pressure (P_{lv})/volume function during a basal cardiac cycle (*top*). Dotted lines marked *a* and *b* represent diastolic and end-systolic pressure/volume functions, respectively, in isometric conditions: I, filling phase; II, isometric contraction; III, ejection phase; IV, isometric relaxation. *Middle*: time pattern of systemic arterial pressure (continuous line) and P_{lv} (dashed line). *Bottom*: time pattern of cardiac output (CO) from left ventricle.

Carotid Baroreflex

When the operation of the carotid baroreflex is described, a distinction is made among the afferent pathway (involving the carotid baroreceptors and the sinus nerve), the efferent sympathetic and parasympathetic pathways, and the action of several distinct effectors; these represent the response to sympathetic stimulation of the peripheral systemic resistances (both splanchnic and extrasplanchnic), of systemic venous unstressed volumes (both splanchnic and extrasplanchnic), and of heart contractility (E_{max}, in both left and right ventricles) and the response of heart period to both sympathetic and vagal activities. A systemic venous compliance control mechanism included in a previous paper (47) has not been explicitly considered here, because it plays a minor role (42).

Afferent pathway. The dynamic relationship between intrasinus pressure and the activity of the sinus nerves is described according to experimental results reported in the recent physiological literature (6, 24). Two main aspects arising from these experiments are considered. First, the relationship between intrasinus pressure and sinus nerve activity in static conditions exhibits a sigmoidal shape with upper saturation and lower threshold. This relationship is observed in experiments in which the carotid sinuses are loaded with a static pressure (6). Second, the carotid sinus baroreceptors are sensitive not only to the intrasinus pressure mean value but also to its rate of change (6, 24). These two properties have been reproduced by representing the carotid baroreceptor plus the afferent pathway as a first-order linear differential equation, with a static gain and a rate-dependent gain, connected in series with a sigmoidal static function.

Efferent sympathetic and parasympathetic (vagal) pathways. Increasing the frequency of spikes in the sinus nerve results in a decrease in the frequency of the sympathetic fibers and in an increase in vagal activity. These relationships have been reproduced by using a monotonically decreasing monoexponential static curve for the sympathetic efferent activity (48) and a monotonically increasing exponential curve, with upper saturation, for the vagal activity (21). A possible pure delay introduced by processing in the central neural system has been neglected, because it can be considered part of the dynamic response of the effectors.

Effector responses to sympathetic activity. All the effectors in the model change in response to stimulation of sympathetic nerves. The response of a generic effector to sympathetic stimulation includes a pure delay, a monotonic logarithmic static function, and a linear first-order dynamics with a real time constant. The presence of pure delays in the responses is largely documented in the physiological literature (10, 21, 33, 37); moreover, delays play a pivotal role in affecting the stability margin of the overall system and might be involved in the generation of Mayer waves (18). The use of logarithmic relationships is justified because the effector static response exhibits a rapid slope at low sympathetic frequencies and then progressively flattens (20, 26). Of course, the static function is monotonically increasing when the peripheral systemic resistances and the end-systolic elastances are considered but monotonically decreasing when heart period and systemic venous unstressed volumes are considered. Finally, the first-order dynamics simulates the time required for the effector to progressively complete its action.

Effector response: Sympathovagal control of heart period. Heart period in the model is affected not only by the sympathetic but also by the vagal activity. The response to vagal stimulation also includes a pure delay, a monotonic static function, and a first-order linear dynamics. However, according to data reported by Parker et al. (30) and Katona et al. (21), I assumed that the static relationship is linear, i.e., heart period increases proportionally to vagal stimulation. The final heart period level is then computed by summing the positive changes induced by the vagal stimulation, the negative changes induced by the sympathetic stimulation, and a constant level representing heart period in the absence of cardiac innervation. Hence, the two mechanisms interact linearly in the heart period control. Of course, this is a crude simplification of the real sympathetic-parasympathetic interaction. However, as shown in RESULTS, it provides an acceptable approximation of heart rate changes under a variety of physiological conditions.

PARAMETER ASSIGNMENT

All parameters in the model have values taken from the literature, suitably rescaled for a subject with a 70-kg body weight.

Vascular System

Values for the compliances and inertances in large systemic and pulmonary arteries have been assigned according

Downloaded from http://ajpheart.physiology.org/ by 10.220.33.2 on September 9, 2017

to previously reported data (3). Resistances in the systemic and pulmonary arteries have been given to reproduce the aortic and pulmonary input impedance in the midfrequency range (29).

The parameters in the peripheral and venous compartments (hydraulic resistances, compliances, and unstressed volumes) have been derived from a previous paper (47), in which a detailed analysis can be found. A division between the splanchnic and extrasplanchnic circulation has been carried out assuming that normal blood flow in the splanchnic circulation is as high as 1.6 l/min (36) (i.e., ~30% of cardiac output) and using values of compliance and total blood volume in the splanchnic circulations that agree with Donald (9), Greenway and Lister (16), and Rothe (34). Moreover, I assumed that both the splanchnic and the extrasplanchnic circulations exhibit the same ratios between venous and arterial quantities adopted previously for the whole systemic circulation. Values for all parameters for the vascular system under basal conditions are shown in Table 1.

Heart

Values for the compliances and unstressed volumes in the left and right atria and the resistances of the atrioventricular valves have been assigned to obtain time patterns of atrial pressures and volumes in agreement with those reported previously (29). Values for the parameters describing the end-diastolic pressure-volume relationship in the left ventricle [($P_{0,lv}$) and ($k_{E,lv}$); see *Eq. 18* in APPENDIX] have been assigned from data measured by Gaasch et al. (14) in human subjects. The same parameters for the right heart ($P_{0,rv}$ and $k_{E,rv}$) have been computed starting from Janicki and Weber (19).

Values for the parameters that mimic the viscosity of the ventricles ($k_{R,lv}$ and $k_{R,rv}$ in *Eqs. 16* and *27* in APPENDIX) have been drawn from experiments performed on dogs (5, 44) and suitably rescaled to reflect that the canine ventricle volume is only about one-third to one-fourth of that in human beings.

Values for the parameters describing the end-systolic pressure/volume function of the left ventricle ($E_{max,lv}$ and $V_{u,lv}$, see *Eq. 18*) have been derived from data measured in humans (2, 46). I am not aware of clinical data obtained in human subjects concerning the same parameters ($E_{max,rv}$ and $V_{u,rv}$) of the right ventricle. Hence, I refer here to the data reported in Janicki and Weber (19) and Maughan et al. (27) for the dog. These data suggest the following ratios between parameters in the right and left ventricle: $E_{max,rv}/E_{max,lv} = 0.59$; $V_{u,rv}/V_{u,lv} = 2.45$. The same ratios have also been deemed valid for humans in basal conditions.

Table 1. *Parameters characterizing the vascular system in basal condition*

Compliance, ml/mmHg	Unstressed Volume, ml	Hydraulic Resistance, mmHg·s·ml^{-1}	Inertance, mmHg·ml·s^{-2}
$C_{sa} = 0.28$	$V_{u,sa} = 0$	$R_{sa} = 0.06$	$L_{sa} = 0.22 \cdot 10^{-3}$
$C_{sp} = 2.05$	$V_{u,sp} = 274.4$	$R_{sp} = 3.307$	
$C_{ep} = 1.67$	$V_{u,ep} = 336.6$	$R_{ep} = 1.407$	
$C_{sv} = 61.11$	$V_{u,sv} = 1{,}121$	$R_{sv} = 0.038$	
$C_{ev} = 50.0$	$V_{u,ev} = 1{,}375$	$R_{ev} = 0.016$	
$C_{pa} = 0.76$	$V_{u,pa} = 0$	$R_{pa} = 0.023$	$L_{pa} = 0.18 \cdot 10^{-3}$
$C_{pp} = 5.80$	$V_{u,pp} = 123$	$R_{pp} = 0.0894$	
$C_{pv} = 25.37$	$V_{u,pv} = 120$	$R_{pv} = 0.0056$	

Total blood volume is 5,300 ml. C, compliance; V_u, unstressed volume; *R*, hydraulic resistance; *L*, inertance. Subscripts: sa, systemic arterial; sp, splanchnic peripheral; ep, extrasplanchnic peripheral; sv, splanchnic venous; ev, extrasplanchnic venous; pa, pulmonary arterial; pp, pulmonary peripheral; pv, pulmonary venous.

Table 2. *Parameters describing the right and left heart*

Left Heart	Right Heart
$C_{la} = 19.23$ ml/mmHg	$C_{ra} = 31.25$ ml/mmHg
$V_{u,la} = 25$ ml	$V_{u,ra} = 25$ ml
$R_{la} = 2.5 \cdot 10^{-3}$ mmHg·s·ml^{-1}	$R_{ra} = 2.5 \cdot 10^{-3}$ mmHg·s·ml^{-1}
$P_{0,lv} = 1.5$ mmHg	$P_{0,rv} = 1.5$ mmHg
$k_{E,lv} = 0.014$ ml^{-1}	$k_{E,rv} = 0.011$ ml^{-1}
$V_{u,lv} = 16.77$ ml	$V_{u,rv} = 40.8$
$E_{max,lv} = 2.95$ mmHg/ml	$E_{max,rv} = 1.75$ mmHg/ml
$k_{R,lv} = 3.75 \cdot 10^{-4}$ s/ml	$k_{R,rv} = 1.4 \cdot 10^{-3}$ s/ml

Basal heart period (*T*) is 0.833 s; k_{sys} and $T_{sys,0}$, which describe duration of systole as function of heart rate, are 0.075 s^2 and 0.5 s, respectively. *R*, resistance of atrioventricular valve; k_E and P_0, parameters describing end-diastolic pressure-volume function of ventricle; E_{max}, slope of end-systolic relationship; k_R, parameter describing dependence of ventricle resistance on isometric pressure. Subscripts: la, left atrium; ra, right atrium; lv, left ventricle; rv, right ventricle.

The basal value of heart rate has been taken as high as 1.2 Hz (72 beats/min), which corresponds to a heart period of 0.833 s. The parameters that provide a value for the duration of systole as a function of heart rate ($T_{sys,0}$ and k_{sys} in *Eq. 22*, APPENDIX) have been taken from data reported in Weissler et al. (49). Values for all parameters for the heart under basal conditions are shown in Table 2.

Afferent Pathway

The parameters in the sigmoidal function are given according to data obtained by Chapleau and Abboud (6) in nonpulsatile conditions and assuming that the central point lies at 92 mmHg. The static and rate-dependent gains in the differential equation have been given according to data obtained by Kubota et al. (24) via white noise stimulation of the carotid baroreceptors and data obtained by Chapleau and Abboud (6) through pulsatile perfusion of the carotid sinuses.

Efferent Sympathetic and Vagal Activities

Parameters describing the sympathetic efferent activity have been given to simulate the percent decrease in the frequency of the sympathetic renal nerve measured by Wang et al. (48) in the dog in response to electrical stimulation of the carotid sinus nerve. Parameters describing the vagal response are difficult to obtain from experiments (21) because the vagus carries not only efferent information but also afferent information coming from the aortic and cardiopulmonary baroreceptors. Hence, parameters describing efferent vagal activity have been given indirectly, to mimic the early heart period response measured in humans through neck chamber maneuvers (12, 13).

Effectors

Parameters of the different effectors are considered separately below.

Contractility. The static contractility control parameters have been based on data reported in Suga et al. (45), Sheriff et al. (40), and Sagawa et al. (38). These data suggest that the slope of the end-systolic pressure/volume function in the vagotomized dog changes by ~33% of the basal level when carotid sinus pressure is altered between 200 and 50 mmHg. A similar percent change has also been assumed for elastance control in the right ventricle. The dynamic parameters (pure delay and time constant) have been set to approximately reproduce the frequency dependence of the open-loop transfer

Downloaded from http://ajpheart.physiology.org/ by 10.220.33.2 on September 9, 2017

Table 3. *Basal values of parameters for regulatory mechanisms*

Parameter Values			
Carotid sinus afferent pathway (Eqs. 30–31)			
$P_n = 92$ mmHg	$f_{min} = 2.52$ spikes/s		$f_{max} = 47.78$ spikes/s
$k_a = 11.758$ mmHg	$\tau_z = 6.37$ s		$\tau_p = 2.076$ s
Sympathetic efferent pathway (Eq. 33)			
$f_{es,\infty} = 2.10$ spikes/s	$f_{es,0} = 16.11$ spikes/s		$k_{es} = 0.0675$ s
	$f_{es,min} = 2.66$ spikes/s		
Vagal efferent pathway (Eq. 34)			
$f_{ev,0} = 3.2$ spikes/s	$f_{ev,\infty} = 6.3$ spikes/s		$k_{ev} = 7.06$ spikes/s
	$f_{cs,0} = 25$ spikes/s		
Effectors (Eqs. 35–42)			
$G_{E_{max,lv}} = 0.475$ mmHg·ml^{-1}·ν^{-1}	$\tau_{E_{max,lv}} = 8$ s	$D_{E_{max,lv}} = 2$ s	$E_{max_{lv,0}} = 2.392$ mmHg/ml
$G_{E_{max,rv}} = 0.282$ mmHg·ml^{-1}·ν^{-1}	$\tau_{E_{max,rv}} = 8$ s	$D_{E_{max,rv}} = 2$ s	$E_{max_{rv,0}} = 1.412$ mmHg/ml
$G_{R,sp} = 0.695$ mmHg·s·ml^{-1}·ν^{-1}	$\tau_{R,sp} = 6$ s	$D_{R,sp} = 2$ s	$R_{sp,0} = 2.49$ mmHg·s·ml^{-1}
$G_{R,ep} = 0.53$ mmHg·s·ml^{-1}·ν^{-1}	$\tau_{R,ep} = 6$ s	$D_{R,ep} = 2$ s	$R_{ep,0} = 0.78$ mmHg·s·ml^{-1}
$G_{V_{u,sv}} = -265.4$ ml/ν	$\tau_{V_{u,sv}} = 20$ s	$D_{V_{u,sv}} = 5$ s	$V_{u_{sv,0}} = 1435.4$ ml
$G_{V_{u,ev}} = -132.5$ ml/ν	$\tau_{V_{u,ev}} = 20$ s	$D_{V_{u,ev}} = 5$ s	$V_{u_{ev,0}} = 1537$ ml
$G_{T,s} = -0.13$ s/ν	$\tau_{T,s} = 2$ s	$D_{T,s} = 2$ s	$T_0 = 0.58$ s
$G_{T,v} = 0.09$ s/ν	$\tau_{T,v} = 1.5$ s	$D_{T,v} = 0.2$ s	

G, mechanism strength; *f*, frequency; τ, time constant; *D*, time delay; *ν*, spikes/s (neural efferent rate). Subscript 0 indicates parameter in absence of innervation (i.e., when vagal and sympathetic activities are zero). Heart period control includes both sympathetic (subscript s) and vagal (subscript v) dependence.

function from carotid sinus pressure to end-systolic elastance estimated by Kubota et al. (23).

Resistance. The gain factors in the static logarithmic relationship have been given according to data reported in Shoukas and Brunner (42) and Potts et al. (32). These authors indicate that total systemic resistance in vagotomized animals increases by ~200–210% when carotid sinus pressure is lowered from 200 to 50 mmHg. However, resistance control seems to be a little weaker in the splanchnic than in the extrasplanchnic circulation (4, 8). Various data suggest that the increase in the splanchnic resistance over the whole baroreceptor sensitivity range is only 70% (4, 20, 34). Finally, the time constants of the resistance control have been given the same values used in a previous work (Ref. 47, in which references can be found), and the pure delay was taken from previously reported data (10).

Unstressed volume. The gain factors in the static logarithmic relationship have been given so that the total reflex change in venous unstressed volume is approximately as great as 15 ml/kg (41–43). Moreover, I assumed that the venous unstressed volume control is much stronger in the splanchnic than in the extrasplanchnic circulation. In fact, experiments performed at constant flow and constant venous pressure suggest that activation of the carotid baroreflex can actively reduce splanchnic venous unstressed volume by 10 ml/kg, which is two-thirds of the total reflex response (4, 9). The remaining portion is ascribed to the extrasplanchnic circulation. According to various authors, the time constants and pure delays of the unstressed volume control are higher than in the resistance control (33 and 43).

Heart period. Parameters that characterize the static effect of vagal and sympathetic activity on heart period have been given to simulate experimental data reported by Levy and Zieske (26). These authors measured heart rate changes in the dog, using different combinations of vagal and sympathetic stimulation. Values for the time constants and pure delays have been given considering that the vagus control is extremely rapid (a few tenths of a second, i.e., it occurs on a beat-by-beat basis), whereas the sympathetic control is characterized by slower dynamics (a few seconds) (21). Values for all parameters concerning the baroreflex control are shown in Table 3.

RESULTS

Numerical integration of differential equations was performed using the fifth-order Runge-Kutta-Fehlberg method with adjustable step length with the software package SIMNON (SIMNON/PCW for Microsoft Windows, version 2.01, SSPA Maritime Consulting, Göteborg, Sweden) devoted to the simulation of ordinary differential equations.[1] Throughout the simulations, the integration and memorization steps were as low as 0.01 s and the error tolerance was set at 1×10^{-6}. Although the model is pulsatile in nature, in Figs. 3–9 only the mean value of the hemodynamic quantities is shown. The mean values were computed from the pulsating quantities by storing a 20-s tracing in stationary conditions (i.e., after the dynamic response to a perturbation has exhausted) and then automatically selecting an integer number of heart periods. The time average of these waveforms was computed using the trapezoidal integration method.

Afferent Pathway

The top panel of Fig. 3 shows the static sigmoidal characteristic of the carotid baroreceptors and the effect of shifting from nonpulsatile to pulsatile loading in the model and in the experiments by Chapleau and Abboud (6). When the carotid sinuses are loaded with a sinusoidal pulsating pressure, the relationship linking

[1] All simulation programs, written according to the software package SIMNON, are available, free of charge, by writing to the author. These programs can be used with SIMNON/PCW version 2.0 or higher.

Downloaded from http://ajpheart.physiology.org/ by 10.220.33.2 on September 9, 2017

intrasinus pressure to the activity of the sinus nerve is converted from sigmoidal to quasilinear in the central pressure range and exhibits lower sensitivity with greater pulsation amplitude. Furthermore, the modulus and phase of the linear first-order dynamics from carotid sinus pressure to sinus nerve activity are shown in the middle and bottom panels of Fig. 3. Modulus and phase increase with frequency in the midfrequency range, suggesting a derivative nature. Similar patterns were observed by Kubota et al. (24) in the dog, using the white noise stimulation technique (see Figs. 1*C* and 2*C* in Ref. 24).

Sympathovagal Control of Heart Period

A detailed description of the heart rate changes induced by different combinations of vagal and sympathetic stimulation was achieved by Levy and Zieske (26) in the dog (Fig. 4, *top*). These authors observed that, at high levels of vagal activity, sympathetic stimulation has only a minor effect on heart rate. In contrast, at high levels of sympathetic activity, vagal stimulation exerts a maximal control on heart rate. Hence, the authors suggested the existence of a significant nonlinear sympathetic-parasympathetic interaction. As shown in the bottom panel of Fig. 4, however, I was able to reproduce these experimental data quite well with the present model, assuming a simple linear sympathetic-parasympathetic interaction in the control of heart period. Hence, the suggestion is that the nonlinear effects visible in the data can be ascribed merely to the hyperbolic relationship linking heart rate to heart period (i.e., HR = 1/*T*). Nonlinear sympathetic-parasympathetic interactions probably occur at different levels in the neural system; however, their inclusion is not necessary to account for the data by Levy and Zieske (26).

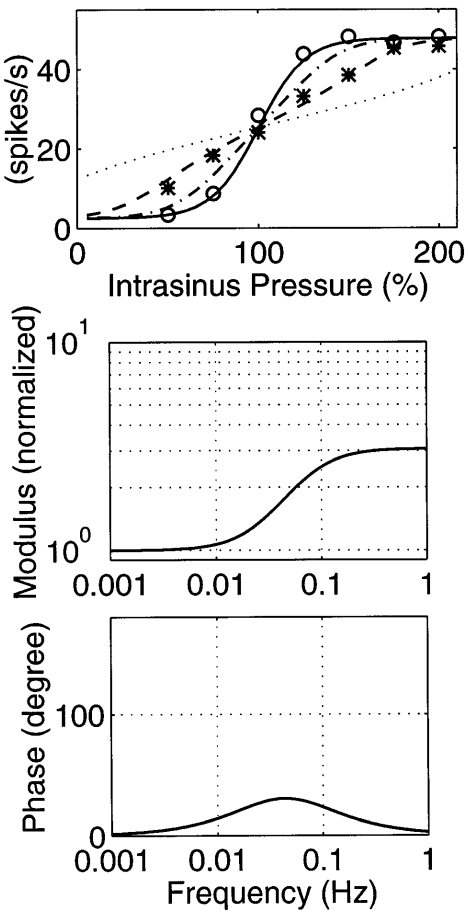

Fig. 3. Main characteristics of afferent pathway from carotid sinus pressure to sinus nerve frequency. *Top*: static sigmoidal carotid baroreceptor function (continuous line) compared with data measured by Chapleau and Abboud (6) in dog with static perfusion of carotid sinuses (○). Effect of a sinusoidal pulsation at carotid sinuses (frequency 1.5 Hz) with different amplitude is also shown (dot-dashed line, 20 mmHg peak to peak; dashed line, 40 mmHg peak to peak; dotted line, 60 mmHg peak to peak) and compared with experimental data obtained by Chapleau and Abboud using 30–50 mmHg peak-to-peak sinusoidal pressure (*). *Middle* and *bottom*: normalized modulus and phase of baroreceptor transfer function in frequency domain.

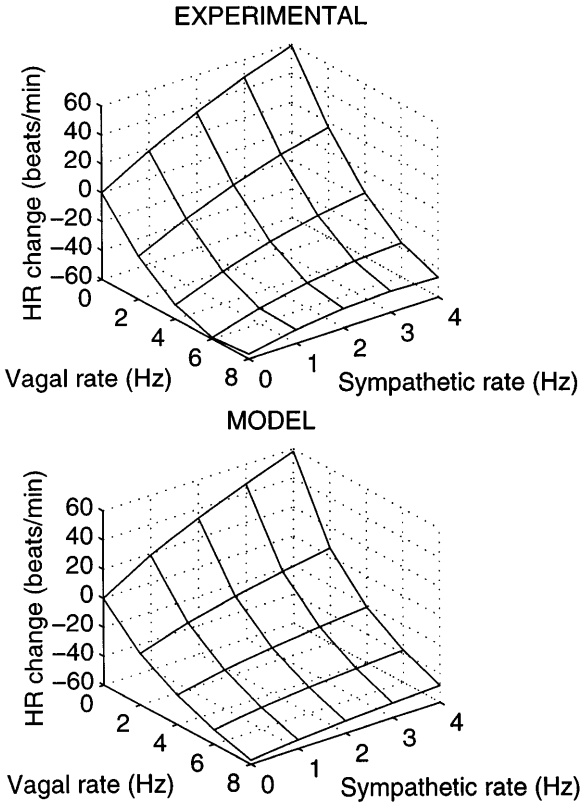

Fig. 4. Effect of combined sympathetic and vagal stimulation, at different frequencies, on heart rate (HR). *Top*: experimental results by Levy and Zieske (26). *Bottom*: model simulation results.

Effect of Carotid Baroreflex on Starling Curve

The Starling curve of the heart was evaluated by giving right atrial pressure different constant values ranging between 1 and 10 mmHg and computing the corresponding values of cardiac output at equilibrium. Evaluation of the Starling curve was then repeated at different intrasinus pressure levels. During all these simulations, systemic arterial pressure was maintained at a constant nonpulsating value (92 mmHg). As a consequence, in this preparation only mechanisms working on heart rate and contractility are functioning

Downloaded from http://ajpheart.physiology.org/ by 10.220.33.2 on September 9, 2017

in open-loop conditions, whereas mechanisms working on resistance (afterload) and unstressed volume (preload) are excluded. This allows the effect of the baroreflex on the Starling curve to be quantified. The simulated dependence of the Starling curve on carotid sinus pressure is shown in the top panel of Fig. 5. As is clear from this figure, reducing carotid sinus pressure causes a significant increase in the flow generation capacity of the heart (in accordance with Refs. 15 and 22). To permit more direct comparison between the model and experimental data, I computed the average percent changes of cardiac output at each intrasinus pressure level. The bottom panel of Fig. 5 shows that there is a rather good quantitative agreement between the model and experimental data, suggesting that the carotid baroreflex mechanisms acting on the heart are adequately simulated.

Artificial Heart Pacing

Several authors speculated that the relationship relating cardiac output to heart rate can be used to characterize the interaction of the heart with the rest of the circulation (see Ref. 28 for review). To simulate the effect of artificial heart pacing on cardiac output, the

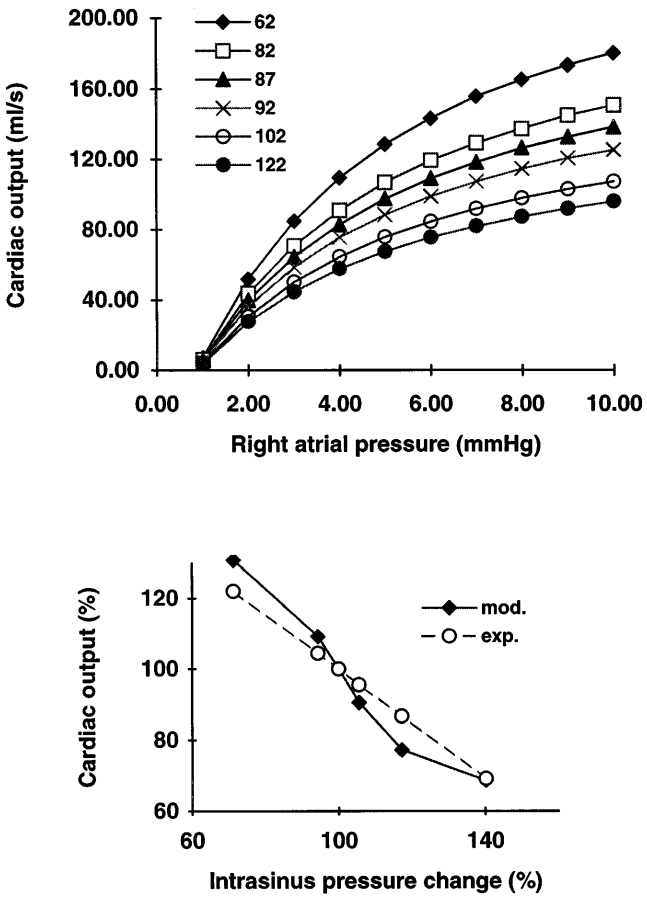

Fig. 5. Effect of carotid baroreflex on Starling curve. *Top*: CO vs. right atrial pressure relationship simulated at constant afterload [systemic arterial pressure (SAP) = 92 mmHg] at different levels of carotid sinus pressure (62, 82, 87, 92, 102, and 122 mmHg). *Bottom*: corresponding average percent changes in CO compared with experimental results by Kostiuk et al. (22) in dog with intact vagus.

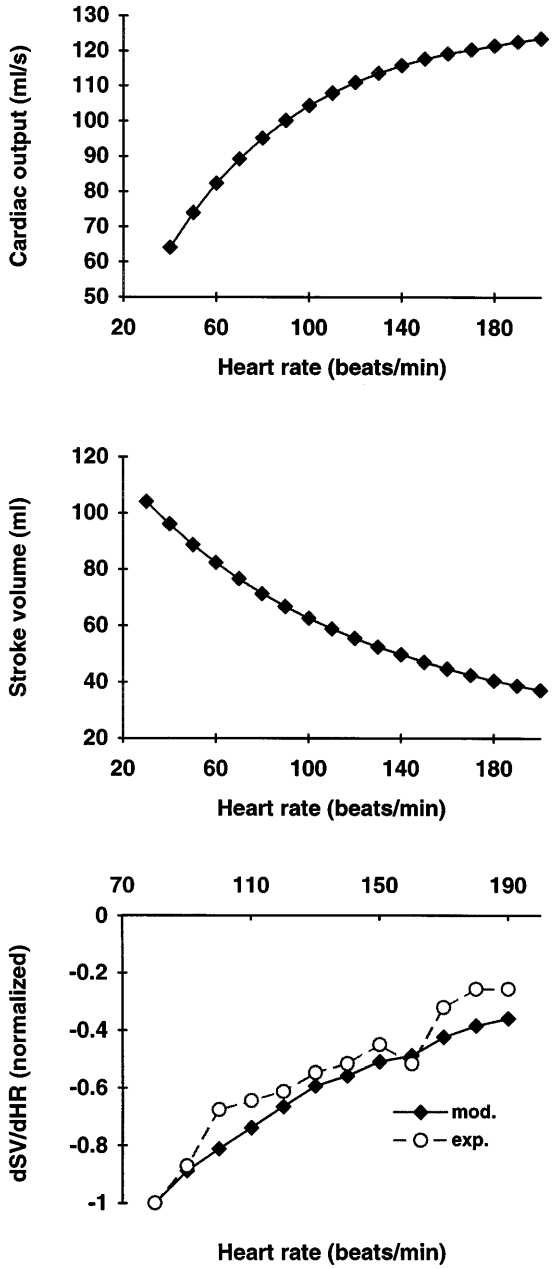

Fig. 6. Effect of heart pacing on CO (*top*) and stroke volume (SV; *middle*). In these simulations feedback loop controlling heart period was broken, and HR was used as an external input. *Bottom*: normalized curve dSV/dHR vs. HR compared with data obtained by Melbin et al. (28) in dog.

feedback loop relating carotid sinus pressure to heart period was cut in the model and heart period was given different values ranging between 30 and 200 beats/min. In this experimental setting all baroreflex regulatory mechanisms are working in closed-loop conditions, with the exception only of the heart rate control. This preparation permits quantification of the heart rate-cardiac output relationship. The top panel of Fig. 6 shows that cardiac output increases with heart rate at the lower heart rate levels and then levels out. At physiological frequencies, cardiac output seems to increase moderately with frequency. The failure of car-

Downloaded from http://ajpheart.physiology.org/ by 10.220.33.2 on September 9, 2017

diac output to further increase at high values of heart rate is a consequence of a decline in ventricular filling, which causes a reduction in end-diastolic volume and hence also in stroke volume (SV) (Fig. 6, *middle*).

The bottom panel of Fig. 6 compares the normalized dSV/dHR vs. HR relationship in the model with that reported in Melbin et al. (Fig. 2 in Ref. 28). Because stroke volume is different in humans and dogs, the two curves were normalized to the value at 80 beats/min. The agreement between the model and the experiments by Melbin et al. is good.

Carotid Baroreflex in Open-Loop Nonpulsatile Conditions

To simulate the carotid baroreflex response in open-loop conditions, carotid sinus pressure in the model was given different constant values ranging between 40 and 150 mmHg and the pattern of the main hemodynamic quantities was computed at equilibrium.

Figure 7 shows blood volume changes in the splanchnic and extrasplanchnic circulations, heart period, systemic resistance, cardiac output, and mean systemic arterial pressure. In the latter cases, simulations have been repeated by eliminating the effect of the vagus [i.e., assuming vagal frequency (f_{ev}) = 0 in the model] to permit better comparison with experimental data in vagotomized animals. In fact, experimental data obtained with the vagus intact cannot be directly compared with model results because of the antagonistic action of the aortic arch. Volume shifts in the splanchnic and extrasplanchnic circulations have been computed by maintaining constant venous pressures and flows, as in the experiment by Brunner et al. (4).

Effect of Intrasinus Pressure Pulsatility

To analyze the role of intrasinus pressure pulsatility on the carotid baroreflex control, pressure at the carotid sinuses was given a sinusoidal pulsatile pattern with various combinations of mean level, amplitude, and frequency of pulsations. The effect of pulsatility on the overall open-loop baroreflex response (mean systemic arterial pressure vs. mean intrasinus pressure) is summarized in Fig. 8 and compared with the experimental results by Schmidt et al. (39). All these figures were obtained using a frequency of 2 Hz. Varying frequency in the range of 1–4 Hz had little effect on the results.

As is clear from the figure, a pulsating pressure at the carotid sinuses decreases the sensitivity of the

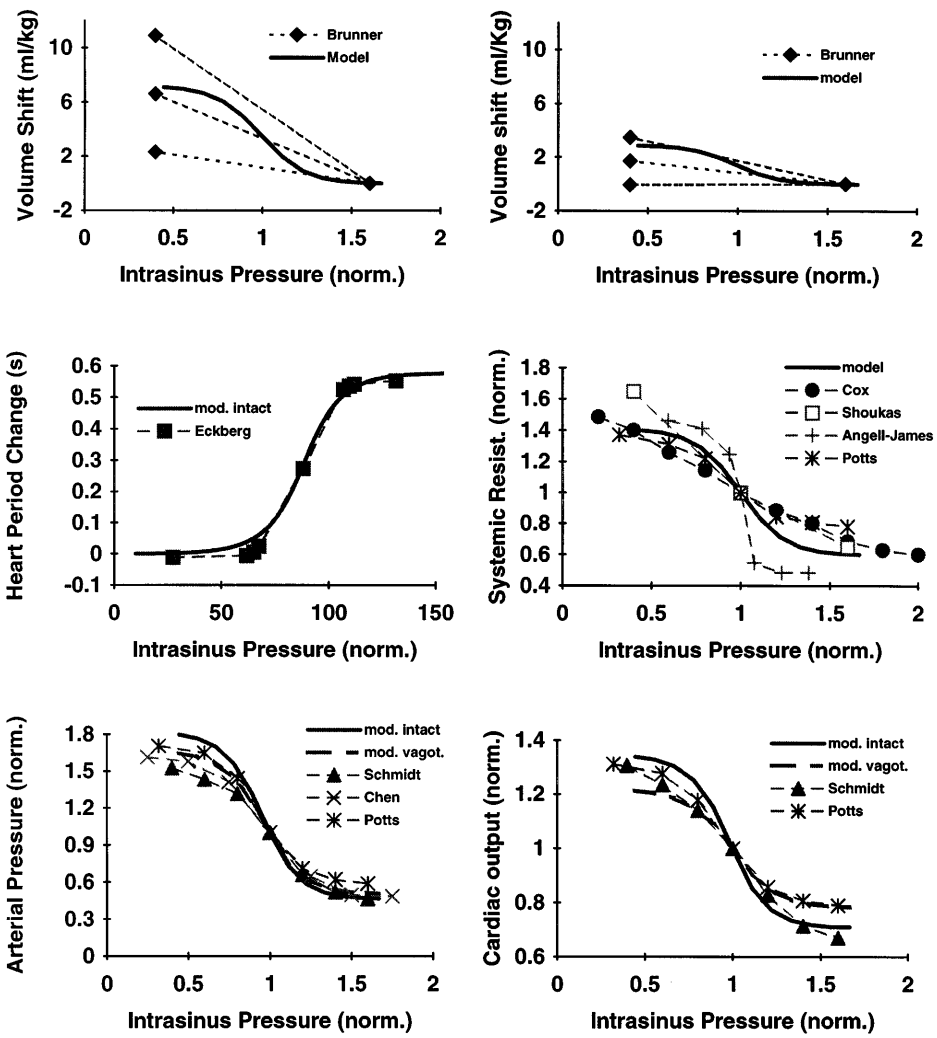

Fig. 7. Summary of carotid baroreflex responses in open-loop conditions with static loading of carotid sinuses. Continuous thick lines are model simulation results. Top 2 panels show blood volume changes in splanchnic (*left*) and extrasplanchnic (*right*) vascular beds, evaluated at constant flow and constant venous pressure; experimental data are means ± SD computed from Fig. 9 in Brunner et al. (4). *Middle left*: comparison of model heart period changes with those measured by Eckberg and Sleight (12, 13) in humans, using neck chamber. *Middle right*: normalized total sytemic resistance in model and in experiments on vagotomized animals (1, 8, 32, 42). *Bottom panels*: patterns of mean SAP and CO. To permit better comparison with experimental data (7, 32, 39) in the last 2 cases, simulations have been repeated in vagotomized conditions (dashed thick lines).

Downloaded from http://ajpheart.physiology.org/ by 10.220.33.2 on September 9, 2017

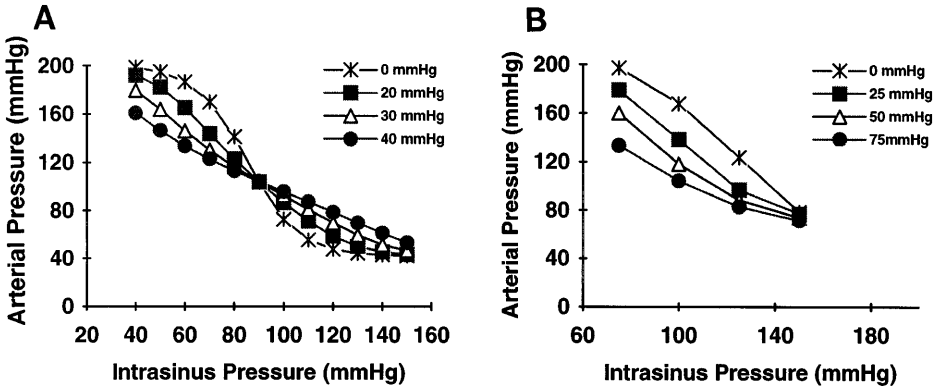

Fig. 8. Effect of pressure-pulse amplitude at carotid sinuses on overall open-loop characteristic of baroreflex. During these simulations (*A*), a sinusoidal pulsating pressure (frequency 2 Hz) with different peak-to-peak amplitudes (0, 20, 30, and 40 mmHg) was superimposed at different carotid sinus pressure mean levels. Pulsating pressure depresses carotid baroreflex gain. By way of comparison, results by Schmidt et al. (39) are shown (*B*).

carotid baroreflex and moves the region of maximum gain toward lower arterial pressure values. Moreover, the pulsatility effect depends significantly on the intrasinus pressure mean level. The effect of pulsatility is quite negligible when mean intrasinus pressure lies in the central linear range. In contrast, pulsatility has the maximum effect when the mean pressure level is located in the nonlinear region of the static characteristic.

Acute Hemorrhage

To test model behavior in closed-loop conditions, I simulated the effect of an acute blood volume loss (−10% of total) performed in 5 s, with all mechanisms working in closed-loop condition. The percent changes in mean systemic arterial pressure, cardiac output, total systemic resistance, and heart rate have been computed after 80 s from the perturbation. The simulation results, shown in the top panel of Fig. 9, are compared with the results obtained by Kumada et al. (25) in the intact dog. The agreement is quite satisfactory. It is worth noting that frequency increases less in the model than in the experimental data. This discrepancy might be imputed to the effect of the aortic arch baroregulation or chemoreceptors.

A sensitivity analysis of the role of the different effectors after acute hemorrhage is presented in the bottom panel of Fig. 9. In this analysis, the strength of each mechanism has been individually lowered down to zero, whereas the remaining mechanisms are working normally. The results suggest that control of venous unstressed volume plays the major role in maintaining cardiac output and systemic arterial pressure in the early phase after hemorrhage, whereas the systemic resistance and heart rate controls are a little less important. Finally, the control of cardiac elastance seems to play a minor role in the response to hemorrhage.

DISCUSSION

The model presented in this paper represents an effort to integrate the various known mechanisms of the carotid baroreflex, often considered separately, into a comprehensive theoretical setting. I feel that this kind of synthesis is urgently needed, because the large quantities of data accumulated in recent years run the risk of being insufficiently exploited if the mutual relationships and reciprocal associations are not clearly pointed out. Single experimental results acquire greater meaning if they are inserted into a more general theoretical vision, in which they are related with other data and can be used to confirm, modify, or contradict previous established knowledge. In this way, the present model aspires to represent the carotid baroreflex as the combination of several distinct parts, each with its own characteristics, that interact nonlinearly and whose

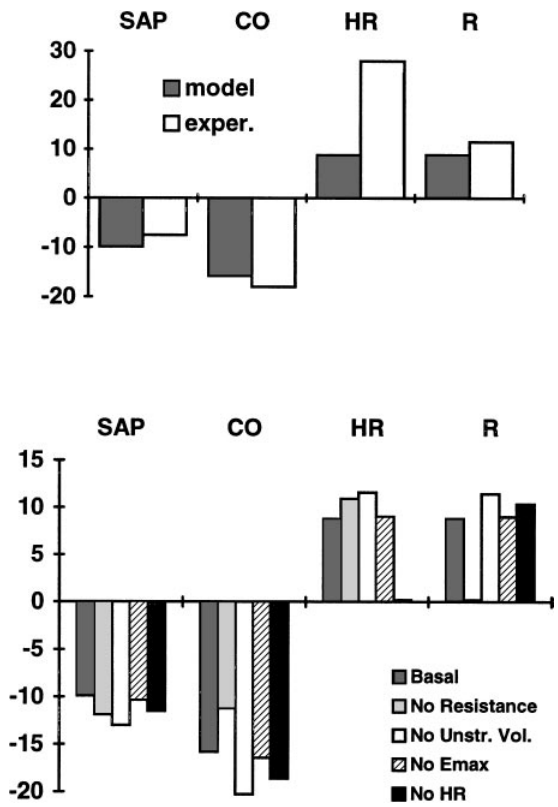

Fig. 9. *Top*: percent changes in mean value of main hemodynamic quantities [SAP, CO, peripheral systemic resistance (*R*), HR] caused by acute hemorrhage (−10% of total blood volume). Simulation results (model) were evaluated at 80 s after hemorrhage and compared with results obtained by Kumada et al. (25) in intact dog (exper). *Bottom*: sensitivity analysis of role of the 4 effectors. Strength of mechanisms working on different effectors [*R*, end-systolic elastance (E_{max}), venous unstressed volume, and HR] was individually reduced to zero, still preserving same initial basal condition. Percent changes in SAP, CO, *R*, and HR after acute hemorrhage (−10% of total blood volume) were then reevaluated and compared with intact case.

Downloaded from http://ajpheart.physiology.org/ by 10.220.33.2 on September 9, 2017

final integration provides the complex kind of regulation experienced in vivo.

An important aspect of the model is the distinction among the different functional parts of the carotid baroreflex, i.e., the afferent pathway including the carotid baroreceptors and sinus nerves, the central neural processing system, and the peripheral effectors. This distinction may enable improved understanding of the possible role of each part in baroregulation and of the consequences of their pathological changes. Moreover, this distinction makes it simpler to refine the model in future work including new aspects not considered here (e.g., the cardiopulmonary and aortic baroafferents).

A new feature of the present model, which distinguishes it from most baroregulation models developed previously, is the characterization of the heart as a pulsatile pump. This choice permits the baroreflex to be studied in its natural working condition, when the carotid pressoreceptors are rhythmically loaded and unloaded by the pulsating sphygmic wave.

Despite the unavoidable limitations involved in modeling a complex physiological system, the model is able to reproduce several aspects of carotid baroreflex control rather well. In the following, I analyze the main perturbations simulated in this work separately and critically comment on the corresponding results.

Sympathovagal Balance

The model assumes the common viewpoint for heart rate control, i.e., heart rate is increased by activation of the sympathetic system during hypotension and decreased by vagal activation during hypertension. Moreover, the two mechanisms superimpose their actions in the central pressure range.

In this model the sympathetic and parasympathetic mechanisms interact linearly in the regulation of heart period. Of course, this is a simplification of the reality, because nonlinearities in the sympathetic-parasympathetic interaction probably occur at different neural levels. However, with this assumption the model allows good reproduction of the experimental findings by Levy and Zieske (26), who observed significant nonlinearities when measuring heart rate as a function of sympathetic and parasympathetic neural activities. Indeed, the present simulations suggest that the significant nonlinearities in the experimental curves are not a consequence of a facilitatory-inhibitory interaction but depend on the hyperbolic nonlinear relationship that holds between heart period (T) and heart rate (HR, = $1/T$). Vagus stimulation moves the working point to a different position on the hyperbolic relationship, characterized by a much smaller slope (dHR/dT). The small slope, in turn, explains the small effect that sympathetic stimulation has on heart rate at high levels of vagal activity.

Changes in Cardiac Function Curve

The simulation results confirm experimental data (15, 22) according to which the carotid baroreflex can significantly affect the cardiac function curve. The model ascribes baroreflex action on the Starling relationship to the combined action of mechanisms working on heart rate and E_{max}.

The results in Fig. 5 were obtained by using constant afterload and preload. In contrast, simulations performed in more physiological conditions, in which mean systemic arterial pressure and atrial pressure are free to vary, show that changes in the pumping ability of the heart may be almost completely masked in vivo by alterations in afterload and, especially, in preload. The effects of changes in preload are evident from the simulation results on atrial pacing and hemorrhage discussed below.

Cardiac Output With Heart Rate Changes

Changes in heart rate have been used in many studies to analyze the relationships of the heart with the rest of the circulatory system (i.e., with preload and afterload). Various authors observed that heart pacing may cause controversial effects on cardiac output; increasing heart rate causes only a moderate increase in cardiac output at physiological levels of heart rate, whereas at high heart rate levels, cardiac output remains unchanged or may even decrease (see Ref. 28).

The results of the present simulation confirm the existence of a different pattern of cardiac output vs. heart rate, depending on ventricular filling and stroke volume. When heart rate lies in the range of 60–90 beats/min, its variations have only a moderate impact on cardiac output (a 30% increase in heart rate causing only 15% increase in cardiac output). When heart rate is >110 beats/min, its changes have less effect on cardiac output.

The moderate effect of heart rate changes on cardiac output visible in Fig. 6 can be ascribed to a decrease in end-diastolic pressure, consequent both on baroreflex control (which causes an increase in venous unstressed volume during heart rate increase) and passive volume redistribution. Of course, these effects were not present in the simulations of Fig. 5, which were performed at constant systemic arterial pressure and constant preload. An important physiological consequence of the results in Fig. 6 is that mechanisms working on heart rate may have a different role in cardiovascular control, depending on the initial heart rate and the availability of venous return. We may expect that, in conditions of poor venous return and/or increased heart rate (such as in vagotomized subjects, in which heart rate is increased far above normal), the reflex mechanisms working on heart period may play a scanty role. In contrast, these mechanisms may have greater importance during bradycardia and/or in conditions characterized by high mean filling pressure.

Recently, Melbin et al. (28) suggested that the relationship linking the dSV/dHR function to HR can be used to predict the cardiac output response to a variety of different perturbations and is thus a useful expression for cardiac function. I tested the ability of the model to predict the dSV/dHR function observed by Melbin et al. during atrial pacing. The good agreement

Downloaded from http://ajpheart.physiology.org/ by 10.220.33.2 on September 9, 2017

obtained in this case suggests that the model may find application, in future studies, in simulating the effect of other perturbations that modify stroke volume (e.g., volume loading or unloading, increase in venous resistance, etc.) to investigate the possible clinical meaning of the dSV/dHR function.

Pressure Pulsatility and Carotid Baroreflex

The results obtained by the present model support the observations of several authors, according to whom shifting from nonpulsatile to pulsatile perfusion of the carotid sinuses at low pressure reduces the mean value of the main hemodynamic quantities and attenuates the baroreflex gain (1, 39). This model result, however, depends crucially on the intrasinus pressure mean value on which pulsations are superimposed. In the present model, the depressive effect of pulsatility can be seen only if mean intrasinus pressure lies below the central point of the static sigmoidal baroreceptor function, a little above the threshold. However, according to the results of Chapleau and Abboud (6), our simulations indicate that pressure pulsatility applied above the central point of the static curve causes a reduction in the activity of the sinus nerve (Fig. 3); hence, in this condition pulsatility might have a hypertensive effect (Fig. 8).

Acute Hemorrhage

The model is able to reproduce the hemodynamic response to acute hemorrhage fairly well by using the basal values of the parameters. Moreover, the sensitivity analysis reveals that control of venous unstressed volume plays the major role in protecting the cardiovascular system in the early phase after acute blood losses. If the unstressed volume control in the model is depressed, we can observe a serious reduction in mean systemic arterial pressure and cardiac output after hemorrhage (Fig. 9). Control of peripheral systemic resistance and heart rate also plays a certain role, but this seems a little less important than the role played by venous unstressed volume.

This result can be justified by examining the relationships among hemodynamic quantities shown in Fig. 9. The main hemodynamic perturbation induced by hemorrhage is a fall in mean systemic filling pressure, which causes a fall in venous return, end-diastolic pressure, and cardiac output. It thus makes sense that this perturbation should be primarily counteracted by venous constriction, which restores mean filling pressure toward more physiological levels without affecting the arteriolar circulation to peripheral organs. This idea is confirmed by the experimental results of Greene and Shoukas (15), who observed that activation of the carotid sinus baroreflex causes large changes in the zero flow intercept of the venous return curve (i.e., in mean circulatory filling pressure) and by Drees and Rothe (11), who measured relevant active changes in mean circulatory filling pressure after hemorrhage in the dog. The reason for the smaller role of systemic resistance regulation after hemorrhage is that, when the heart is partially empty, increasing afterload causes a secondary fall in cardiac output (Fig. 9), which results in only minor benefits on mean systemic arterial pressure. Indeed, we can expect that baroreflex control of systemic resistance plays a major role in response to other hemodynamic perturbations (such as metabolic vasodilation, hypoxia, hypercapnia, and thermal stresses) that primarily affect the cardiac afterload with only secondary changes in preload. Moreover, the baroreflex control of vascular resistance may also become important in the middle period after hemorrhage, by increasing vascular refilling through a reduction in capillary pressure.

Furthermore, the present simulations confirm the observations by others (4, 9, 16), according to whom the splanchnic circulation is responsible for a significant portion of the blood volume shift during baroreflex activation. The model ascribes this behavior mainly to the existence of a stronger venous unstressed volume control in the splanchnic circulation than in the extrasplanchnic circulation. Volume redistribution from arteriolar vasoconstriction (Jager-Krogh phenomenon) appears scarcely important in the model, because the increase in resistance caused by the carotid baroreflex is smaller in the splanchnic than in the extrasplanchnic vessels (4, 8).

Finally, it is important to point out the main limitations and simplifications of the present model, which may be improved in future. A first limitation concerns the absence of local autoregulation mechanisms in the control of peripheral systemic resistance. We can expect that in conditions in which cardiac output and mean systemic arterial pressure decrease significantly (e.g., after acute hemorrhage), the vasoconstrictory action of the carotid baroreflex is counteracted by peripheral vasodilation in the organs (like the brain, heart, and muscles) with a higher metabolic rate.

A second possible shortcoming concerns the dependence of heart contractility on the carotid baroreflex and on other hemodynamic influences. In this study, I took a traditional viewpoint (38) and assumed that the carotid baroreflex acts, through sympathetic activation, only on the slope of the end-systolic pressure/volume function. The results of some experiments, however, cast doubt on this simplification, indicating that vagal stimulation and changes in systemic input impedance might also significantly influence the slope and x-axis intercept of the left ventricle end-systolic relationship. Furthermore, the present model neglects the effect of changes in coronary perfusion on the end-systolic pressure/volume function. These effects, however, may become important if coronary artery pressure is reduced below the autoregulation limit (38).

A further limitation concerns the absence of vagal afferents in the model, especially cardiopulmonary baroreceptors. Their role, however, might be significant in humans in response to some perturbations such as nonhypotensive hemorrhage or mild lower body negative pressure. Moreover, inclusion of vagal baroafferents may be worthwhile to reproduce paradoxical re-

Downloaded from http://ajpheart.physiology.org/ by 10.220.33.2 on September 9, 2017

sponses of the cardiovascular system such as the vasovagal syncope (13).

Perhaps the most far-reaching simplification in the present model concerns the description of the central neural processing system, which was simply mimicked by means of monotonic exponential functions linking activity in the afferent and efferent neural pathways. Increasing evidence has accumulated in recent years on the functional role that the central mechanisms may play in the carotid baroreflex response. This aspect will require new modeling efforts in future years, perhaps using modern neural network computation techniques.

APPENDIX: QUANTITATIVE MODEL DESCRIPTION

The Vascular System

Equations relating pressures and volumes in the different points of the vascular bed can be written by imposing conservation of mass at all compliances of Fig. 1 and balance of forces in the large arteries. P_j is intravascular pressure in the jth compartment, $V_{u,j}$ is the corresponding unstressed volume (defined as the volume at zero pressure), F_j is blood flow, and C_j, L_j, and R_j are compliances, inertances, and hydraulic resistances, respectively. Finally, $F_{o,r}$ and $F_{o,l}$ are cardiac output from the left and right ventricle, respectively.

Conservation of Mass at Pulmonary Arteries (C_{pa})

$$\frac{dP_{pa}}{dt} = \frac{1}{C_{pa}} \cdot (F_{o,r} - F_{pa}) \tag{1}$$

Balance of Forces at Pulmonary Arteries (L_{pa})

$$\frac{dF_{pa}}{dt} = \frac{1}{L_{pa}} \cdot (P_{pa} - P_{pp} - R_{pa} \cdot F_{pa}) \tag{2}$$

Conservation of Mass at Pulmonary Peripheral Circulation (C_{pp})

$$\frac{dP_{pp}}{dt} = \frac{1}{C_{pp}} \left(F_{pa} - \frac{P_{pp} - P_{pv}}{R_{pp}} \right) \tag{3}$$

Conservation of Mass at Pulmonary Veins (C_{pv})

$$\frac{dP_{pv}}{dt} = \frac{1}{C_{pv}} \left(\frac{P_{pp} - P_{pv}}{R_{pp}} - \frac{P_{pv} - P_{la}}{R_{pv}} \right) \tag{4}$$

Conservation of Mass at Systemic Arteries (C_{sa})

$$\frac{dP_{sa}}{dt} = \frac{1}{C_{sa}} \cdot (F_{o,l} - F_{sa}) \tag{5}$$

Balance of Forces at Systemic Arteries (L_{sa})

$$\frac{dF_{sa}}{dt} = \frac{1}{L_{sa}} \cdot (P_{sa} - P_{sp} - R_{sa} \cdot F_{sa}) \tag{6}$$

Conservation of Mass at Peripheral Systemic Circulation (C_{sp} and C_{ep})

$$\frac{dP_{sp}}{dt} = \frac{1}{C_{sp} + C_{ep}} \left(F_{sa} - \frac{P_{sp} - P_{sv}}{R_{sp}} - \frac{P_{sp} - P_{ev}}{R_{ep}} \right) \tag{7}$$

Conservation of Mass at Extrasplanchnic Venous Circulation (C_{ev})

$$\frac{dP_{ev}}{dt} = \frac{1}{C_{ev}} \cdot \left(\frac{P_{sp} - P_{ev}}{R_{ep}} - \frac{P_{ev} - P_{ra}}{R_{ev}} - \frac{dV_{u,ev}}{dt} \right) \tag{8}$$

Finally, pressure in the splanchnic venous circulation is computed by assuming that the total amount of blood volume contained in the circulatory system (V_t) is known. Hence

$$\begin{aligned} P_{sv} = \frac{1}{C_{sv}} [V_t - C_{sa} \cdot P_{sa} - (C_{sp} + C_{ep}) \cdot P_{sp} - C_{ev} \cdot P_{ev} - C_{ra} \cdot P_{ra} \\ - V_{rv} - C_{pa} \cdot P_{pa} - C_{pp} \cdot P_{pp} - C_{pv} \cdot P_{pv} - C_{la} \cdot P_{la} - V_{lv} - V_u] \end{aligned} \tag{9}$$

where V_{rv} and V_{lv} are the volumes contained in the right and left ventricles, respectively (see *The Heart as a Pump*), and V_u is the total unstressed volume, equal to the sum of the unstressed volumes in the different compartments, i.e.

$$\begin{aligned} V_u = + V_{u,sa} + V_{u,sp} + V_{u,ep} + V_{u,sv} + V_{u,ev} + V_{u,ra} \\ + V_{u,pa} + V_{u,pp} + V_{u,pv} + V_{u,la} \end{aligned} \tag{10}$$

V_t may change during simulation as a consequence of transfusion or hemorrhage. A further differential equation can thus be written

$$\frac{dV_t(t)}{dt} = I(t) \qquad V_t(0) = V_{t,0} \tag{11}$$

where $V_{t,0}$ is the amount of blood volume initially contained in the circulation, and $I(t)$ is the blood injection rate (if positive) or the withdrawal rate (if negative).

The Heart as a Pump

P_{la} can be computed by applying conservation of mass. Hence

$$\frac{dP_{la}}{dt} = \frac{1}{C_{la}} \cdot \left(\frac{P_{pv} - P_{la}}{R_{pv}} - F_{i,l} \right) \tag{12}$$

where the first term in brackets is venous return and $F_{i,l}$ denotes blood flow entering the left ventricle. This term depends on the opening of the atrioventricular valve. Hence

$$F_{i,l} = \begin{cases} 0 & \text{if } P_{la} \le P_{lv} \\ \dfrac{P_{la} - P_{lv}}{R_{la}} & \text{if } P_{la} > P_{lv} \end{cases} \tag{13}$$

V_{lv} is computed by applying conservation of mass

$$\frac{dV_{lv}}{dt} = F_{i,l} - F_{o,l} \tag{14}$$

where $F_{o,l}$ is cardiac output from the left ventricle. Cardiac output, in turn, depends on the opening of the aortic valve, assumed to be ideal

$$F_{o,l} = \begin{cases} 0 & \text{if } P_{max,lv} \le P_{sa} \\ \dfrac{P_{max,lv} - P_{sa}}{R_{lv}} & \text{if } P_{max,lv} > P_{sa} \end{cases} \tag{15}$$

where $P_{max,lv}$ is the isometric left ventricle pressure. The viscous resistance of the left ventricle (R_{lv}) is assumed to be

Downloaded from http://ajpheart.physiology.org/ by 10.220.33.2 on September 9, 2017

proportional to the isometric pressure (44), and so it increases significantly during contraction. We can thus write

$$R_{lv} = k_{R,lv} \cdot P_{max,lv} \tag{16}$$

where $k_{R,lv}$ is a constant parameter.

The instantaneous left ventricle pressure can be obtained as the difference between the isometric pressure and viscous losses. One can thus write

$$P_{lv} = P_{max,lv} - R_{lv} \cdot F_{o,l} \tag{17}$$

According to Sagawa et al. (38), I assumed that the isometric pressure/volume function is exponential at diastole, when the ventricle is relaxed, and linear at end systole, when the ventricle is maximally contracted. Hence

$$\begin{aligned} P_{max,lv}(t) = {} & \varphi(t) \cdot E_{max,lv} \cdot (V_{lv} - V_{u,lv}) \\ & + [1 - \varphi(t)] \cdot P_{0,lv} \cdot (e^{k_{E,lv} \cdot V_{lv}} - 1)] \quad 0 \le \varphi(t) \le 1 \end{aligned} \tag{18}$$

where $E_{max,lv}$ is the ventricle elastance at the instant of maximum contraction, $V_{u,lv}$ is the corresponding ventricle unstressed volume (i.e., the x-axis intercept of the end-systolic pressure/volume function), and $P_{0,lv}$ and $k_{E,lv}$ are constant parameters that characterize the monoexponential pressure/volume function at diastole. Finally, $\varphi(t)$ is the ventricle activation function [with $\varphi(t) = 1$ at maximum contraction, $\varphi(t) = 0$ at complete relaxation]. I adopted the simple expression used by Piene (31), i.e., a squared half-sine wave

$$\varphi(t) = \begin{cases} \sin^2\left[\dfrac{\pi \cdot T(t)}{T_{sys}(t)} \cdot u\right] & 0 \le u \le T_{sys}/T \\ 0 & T_{sys}/T \le u \le 1 \end{cases} \tag{19}$$

where T is the heart period, T_{sys} is the duration of systole, and u is a dimensionless variable, ranging between 0 and 1, that represents the fraction of cardiac cycle. The value $u = 0$ is conventionally assumed as the beginning of systole. An expression for $u(t)$ has been obtained, as a function of T, by means of an "integrate and fire" model, i.e.

$$u(t) = \mathrm{frac}\left[\int_{t_0}^{t} \frac{1}{T(\tau)}\, d\tau + u(t_0)\right] \tag{20}$$

where the function "fractional part" [frac( )] resets the variable $u(t)$ to zero as soon as it reaches the value +1. *Equation 20* is equivalent to the use of an additional state variable; in fact

$$\frac{d\xi}{dt} = \frac{1}{T(t)} \quad \text{with} \quad u(t) = \mathrm{frac}(\xi) \tag{21}$$

Finally, T_{sys} decreases linearly with heart rate (49), i.e.

$$T_{sys} = T_{sys,0} - k_{sys} \cdot \frac{1}{T} \tag{22}$$

where $T_{sys,0}$ and k_{sys} are constant parameters.

Equations similar to *Eqs. 12–22* can also be written for the right heart, with different parameters.

Conservation of Mass at Right Atrium

$$\frac{dP_{ra}}{dt} = \frac{1}{C_{ra}} \cdot \left(\frac{P_{sv} - P_{ra}}{R_{sv}} + \frac{P_{ev} - P_{ra}}{R_{ev}} - F_{i,r}\right) \tag{23}$$

Blood Flow Entering Right Ventricle

$$F_{i,r} = \begin{cases} 0 & \text{if } P_{ra} \le P_{rv} \\ \dfrac{P_{ra} - P_{rv}}{R_{ra}} & \text{if } P_{ra} > P_{rv} \end{cases} \tag{24}$$

Conservation of Mass at Right Ventricle

$$\frac{dV_{rv}}{dt} = F_{i,r} - F_{o,r} \tag{25}$$

Cardiac Output From Right Ventricle

$$F_{o,r} = \begin{cases} 0 & \text{if } P_{max,rv} \le P_{pa} \\ \dfrac{P_{max,rv} - P_{pa}}{R_{rv}} & \text{if } P_{max,rv} > P_{pa} \end{cases} \tag{26}$$

Viscous Resistance of Right Ventricle

$$R_{rv} = k_{R,rv} \cdot P_{max,rv} \tag{27}$$

Instantaneous Right Ventricle Pressure

$$P_{rv} = P_{max,rv} - R_{rv} \cdot F_{o,r} \tag{28}$$

Isometric Pressure in Right Ventricle

$$\begin{aligned} P_{max,rv}(t) = {} & \varphi(t) \cdot E_{max,rv} \cdot (V_{rv} - V_{u,rv}) + [1 - \varphi(t)] \\ & \cdot P_{0,rv} \cdot (e^{k_{E,rv} \cdot V_{rv}} - 1) \quad 0 \le \varphi(t) \le 1 \end{aligned} \tag{29}$$

The same expression for $\varphi(t)$ (*Eqs. 19–22*) holds for both the right and left ventricles.

Carotid Baroreflex Control System

Afferent pathway. According to experimental results (6) the afferent baroreflex pathway is described as the series arrangement of a linear derivative first-order dynamic block and a sigmoidal static characteristic

$$\tau_p \cdot \frac{d\tilde{P}}{dt} = P_{cs} + \tau_z \cdot \frac{dP_{cs}}{dt} - \tilde{P} \tag{30}$$

$$f_{cs} = \left[f_{min} + f_{max} \cdot \exp\left(\frac{\tilde{P} - P_n}{k_a}\right)\right] \Big/ \left[1 + \exp\left(\frac{\tilde{P} - P_n}{k_a}\right)\right] \tag{31}$$

where τ_p and τ_z are the time constants for the real pole and the real zero in the linear dynamic block (usually with $\tau_z/\tau_p > 1$), P_{cs} is the carotid sinus pressure, $\tilde{P}$ is the output variable of the linear dynamic block (having the dimension of a pressure), f_{cs} is the frequency of spikes in the afferent fibers, f_{max} and f_{min} are the upper and lower saturation of the frequency discharge, P_n is the value of intrasinus pressure at the central point of the sigmoidal functional, and k_a is a parameter with the dimension of pressure, related to the slope of the static function at the central point. By denoting with G_b the maximum baroreceptor gain, i.e., the gain at the central point, the following expression holds

$$G_b = \left.\frac{\partial f_{cs}}{\partial \tilde{P}}\right|_{\tilde{P} = P_n} \qquad k_a = \frac{f_{max} - f_{min}}{4 \cdot G_b} \tag{32}$$

In closed-loop conditions, carotid sinus pressure is equal to systemic arterial pressure, i.e., $P_{cs} = P_{sa}$. In contrast, P_{cs} is considered a model input during open-loop simulations.

Downloaded from http://ajpheart.physiology.org/ by 10.220.33.2 on September 9, 2017

Efferent sympathetic pathway. The negative monotonic function that relates the activity in the afferent and efferent neural pathways has been given an exponential trend (48). Hence, we have

$$f_{es} = f_{es,\infty} + (f_{es,0} - f_{es,\infty}) \cdot e^{-k_{es} \cdot f_{cs}} \tag{33}$$

where f_{es} is the frequency of spikes in the efferent sympathetic nerves and k_{es}, f_{es0}, and $f_{es\infty}$ are constants (with $f_{es0} > f_{es\infty}$).

Efferent vagal pathway. The efferent vagal activity increases monotonically with the activity in the sinus nerve until an upper saturation is reached. Hence, the following sigmoidal equation has been used

$$f_{ev} = \left[f_{ev,0} + f_{ev,\infty} \cdot \exp\left(\frac{f_{cs} - f_{cs,0}}{k_{ev}}\right)\right] \Big/ \left[1 + \exp\left(\frac{f_{cs} - f_{cs,0}}{k_{ev}}\right)\right] \tag{34}$$

where f_{ev} is the frequency of spikes in the efferent vagal fibers, k_{ev}, $f_{ev,0}$ and $f_{ev,\infty}$ are constant parameters (with $f_{ev,\infty} > f_{ev,0}$), and $f_{cs,0}$ is the central value in *Eq. 31*.

Regulation effectors. The response of the resistances, unstressed volumes, and cardiac elastances to the sympathetic drive includes a pure latency, a monotonic logarithmic static function, and a low-pass first-order dynamics. Hence, the following equations hold

$$\sigma_\theta(t) = \begin{cases} G_\theta \cdot \ln\,[\,f_{es}(t - D_\theta) - f_{es,min} + 1] & \text{if } f_{es} \geq f_{es,min} \\ 0 & \text{if } f_{es} < f_{es,min} \end{cases} \tag{35}$$

$$\frac{d\Delta\theta}{dt}(t) = \frac{1}{\tau_\theta} \cdot (-\Delta\theta(t) + \sigma_\theta(t) \tag{36}$$

$$\theta(t) = \Delta\theta(t) + \theta_0 \tag{37}$$

where θ denotes the generic controlled parameter, σ_θ is the output of the static characteristic, τ_θ and D_θ are the time constants and pure latency, respectively, of the mechanism, $f_{es,min}$ is the minimum sympathetic stimulation (*Eqs. 31–33*), and $\Delta\theta$ is the parameter change caused by sympathetic stimulation. Finally, G_θ is a constant gain factor, positive for mechanisms working on $E_{max,rv}$, $E_{max,lv}$, R_{sp}, and R_{ep} but negative for $V_{u,sv}$ and $V_{u,ev}$.

The response of the heart period includes a balance between the vagal and sympathetic activities. The heart period changes induced by sympathetic stimulation (ΔT_s) are obtained through equations analogous to *Eqs. 35* and *36*. The response to vagal activity differs from the others because heart period increases linearly with the efferent frequency in the vagus (30). Finally, the heart period level is obtained by assuming a linear interaction between the sympathetic and parasympathetic responses. Hence

$$\sigma_{T,s}(t) = \begin{cases} G_{T,s} \cdot \ln\,[f_{es}(t - D_{T,s}) - f_{es,min} + 1] & \text{if } f_{es} \geq f_{es,min} \\ 0 & \text{if } f_{es} < f_{es,min} \end{cases} \tag{38}$$

$$\frac{d\Delta T_s(t)}{dt} = \frac{1}{\tau_{T,s}} \cdot [-\Delta T_s(t) + \sigma_{T,s}(t)] \tag{39}$$

$$\sigma_{T,v}(t) = G_{T,v} \cdot f_{ev}(t - D_{T,v}) \tag{40}$$

$$\frac{d\Delta T_v(t)}{dt} = \frac{1}{\tau_{T,v}} \cdot [-\Delta T_v(t) + \sigma_{T,v}(t)] \tag{41}$$

$$T = \Delta T_s + \Delta T_v + T_0 \tag{42}$$

where the meaning of symbols is the same as in *Eqs. 35* and *36*. In particular, T_0 denotes heart period in the absence of cardiac innervation.

Address for reprint requests: M. Ursino, Dipartimento di Elettronica, Informatica e Sistemistica, Viale Risorgimento 2, I40136, Bologna, Italy.

Received 9 March 1998; accepted in final form 12 June 1998.

REFERENCES

1. **Angell James, J. E., and M. de Burgh Daly.** Effects of graded pulsatile pressure on the reflex vasomotor responses elicited by changes of mean pressure in the perfused carotid sinus-aortic arch regions of the dog. *J. Physiol. (Lond.)* 214: 51–64, 1971.
2. **Asanoi, H., S. Sasayama, and T. Kameyama.** Ventriculoarterial coupling in normal and failing heart in humans. *Circ. Res.* 65: 483–493, 1989.
3. **Beneken, J. E. W., and B. De Wit.** A physical approach to hemodynamic aspects of the human cardiovascular system. In: *Physical Bases of Circulatory Transport: Regulation and Exchange*, edited by E. B. Reeve and A. C. Guyton. Philadelphia, PA: Saunders, 1967, p. 1–45.
4. **Brunner, M. J., A. A. Shoukas, and C. L. MacAnespie.** The effect of the carotid sinus baroreceptor reflex on blood flow and volume redistribution in the total systemic vascular bed. *Circ. Res.* 48: 274–285, 1981.
5. **Campbell, K. B., J. A. Ringo, Y. Wakao, P. A. Klavano, and J. E. Alexander.** Internal capacitance and resistance allow prediction of right ventricle outflow. *Am. J. Physiol.* 243 (*Heart Circ. Physiol.* 12): H99–H112, 1982.
6. **Chapleau, M. W., and F. M. Abboud.** Contrasting effects of static and pulsatile pressure on carotid baroreceptor activity in dogs. *Circ. Res.* 61: 648–658, 1987.
7. **Chen, H. I., C. Y. Chai, C. S. Tung, and H. C. Chen.** Modulation of the carotid baroreflex function during volume expansion. *Am. J. Physiol.* 237 (*Heart Circ. Physiol.* 6): H153–H158, 1979.
8. **Cox, R. H., and R. J. Bagshaw.** Baroreceptor reflex control of arterial hemodynamics in the dog. *Circ. Res.* 37: 772–786, 1975.
9. **Donald, D. E.** Splanchnic circulation. In *Handbook of Physiology. The Cardiovascular System. Peripheral Circulation and Organ Blood Flow*. Bethesda, MD: Am. Physiol. Soc., 1983, sect. 2, vol. III, pt. 1, chapt. 7, p. 219–240.
10. **Donald, D. E., and A. J. Edis.** Comparison of aortic and carotid baroreflexes in the dog. *J. Physiol. (Lond.)* 215: 521–538, 1971.
11. **Drees, J. A., and C. F. Rothe.** Reflex venoconstriction and capacity vessel pressure-volume relationship in dogs. *Circ. Res.* 34: 360–373, 1974.
12. **Eckberg, D. L.** Nonlinearities of the human carotid broreceptor-cardiac reflex. *Circ. Res.* 47: 208–216, 1980.
13. **Eckberg, D. L., and P. Sleight.** *Human Baroreflexes in Health and Disease*: Oxford, UK: Oxford Univ. Press, 1992.
14. **Gaasch, W. H., H. J. Levine, M. A. Quinones, and J. K. Alexander.** Left ventricular compliance: mechanisms and clinical implications. *Am. J. Cardiol.* 38: 645–653, 1976.
15. **Greene, A. S., and A. A. Shoukas.** Changes in canine cardiac function and venous return curves by the carotid baroreflex. *Am. J. Physiol.* 251 (*Heart Circ. Physiol.* 20): H288–H296, 1986.
16. **Greenway, C. V., and G. E. Lister.** Capacitance effects and blood reservoir function in the splanchnic vascular bed during non-hypotensive haemorrhage and blood volume expansion in anaesthetized cats. *J. Physiol. (Lond.)* 237: 279–294, 1974.
17. **Greenway, C. V., and G. D. Scott.** Quantitative integration of the cardiovascular system and synthesis of drug actions: another attempt. *Can. J. Physiol. Pharmacol.* 68: 1299–1307, 1990.
18. **Hatakeyama, I.** Analysis of baroreceptor control of the circulation. *In Physical Bases of Circulatory Transport: Regulation and Exchange*, edited by E. B. Reeve and A. C. Guyton. Philadelphia, PA: Saunders, 1967, p. 91–112.
19. **Janicki, J. S., and K. T. Weber.** The pericardium and ventricular interaction, distensibility, and function. *Am. J. Physiol.* 238 (*Heart Circ. Physiol.* 7): H494–H503, 1980.

Downloaded from http://ajpheart.physiology.org/ by 10.220.33.2 on September 9, 2017

20. **Karim, F., and R. Hainsworth.** Responses of abdominal vascular capacitance to stimulation of splanchnic nerves. *Am. J. Physiol.* 231: 434–440, 1976.
21. **Katona, P. G., J. W. Poitras, G. O. Barnett, and B. S. Terry.** Cardiac vagal efferent activity and heart period in the carotid sinus reflex. *Am. J. Physiol.* 218: 1030–1037, 1970.
22. **Kostiuk, D. P., K. Sagawa, and A. A. Shoukas.** Modification of the flow-generating capability of the canine heart-lung compartment by the carotid sinus baroreceptor reflex. *Circ. Res.* 38: 546–553, 1976.
23. **Kubota, T., J. Alexander, R. Itaya, K. Todaka, M. Sugimachi, K. Sunagawa, Y. Nose, and A. Takeshita.** Dynamic effects of carotid sinus baroreflex on ventriculoarterial coupling studied in anesthetized dogs. *Circ. Res.* 70: 1044–1053, 1992.
24. **Kubota, T., H. Chishaki, T. Yoshida, K. Sunagawa, A. Takeshita, and Y. Nose.** How to encode arterial pressure into carotid sinus nerve to invoke natural baroreflex. *Am. J. Physiol.* 263 (*Heart Circ. Physiol.* 32): H307–H313, 1992.
25. **Kumada, M., R. M. Schmidt, K. Sagawa, and K. S. Tan.** Carotid sinus reflex in response to hemorrhage. *Am. J. Physiol.* 219: 1373–1379, 1970.
26. **Levy, M. N., and H. Zieske.** Autonomic control of cardiac pacemaker activity and atrioventricular transmission. *J. Appl. Physiol.* 27: 465–470, 1969.
27. **Maughan, W. L., K. Sunagawa, and K. Sagawa.** Ventricular systolic interdependence: volume elastance model in isolated canine hearts. *Am. J. Physiol.* 253 (*Heart Circ. Physiol.* 22): H1381–H1390, 1987.
28. **Melbin, J., D. K. Detweiler, R. A. Riffle, and A. Noordergraaf.** Coherence of cardiac output with rate changes. *Am. J. Physiol.* 243 (*Heart Circ. Physiol.* 12): H499–H504, 1982.
29. **Milnor, W. R.** *Hemodynamics.* Baltimore, MD: Williams and Wilkins, 1982.
30. **Parker, P., B. G. Celler, E. K. Potter, and D. I. McCloskey.** Vagal stimulation and cardiac slowing. *J. Auton. Nerv. Syst.* 11: 226–231, 1984.
31. **Piene, H.** Impedance matching between ventricle and load. *Ann. Biomed. Eng.* 12: 191–207 1984.
32. **Potts, J. T., T. Hatanaka, and A. A. Shoukas.** Effect of arterial compliance on carotid sinus baroreceptor reflex control of the circulation. *Am. J. Physiol.* 270 (*Heart Circ. Physiol.* 39): H988–H1000, 1996.
33. **Rothe, C. F.** Venous system: physiology of the capacitance vessels. In: *Handbook of Physiology. The Cardiovascular System. Peripheral Circulation and Organ Blood Flow*. Bethesda, MD: Am. Physiol. Soc., 1983, sect. 2, vol. III, pt. 1, chapt. 13, p. 397–452.
34. **Rothe, C. F.** Reflex control of veins and vascular capacitance. *Physiol. Rev.* 63: 1281–1342, 1983.
35. **Rothe, C. F.** A simulation package to help learning. *Comput. Life Sci. Educ.* 4: 49–53, 1987.
36. **Rowell, L. B., J. R. Detry, J. R. Blackmon, and C. Wyss.** Importance of the splanchnic vascular bed in human blood pressure regulation. *J. Appl. Physiol.* 32: 213–220, 1972.
37. **Sagawa, K.** Baroreflex control of systemic arterial pressure and vascular bed. In: *Handbook of Physiology: The Cardiovascular System. Peripheral Circulation and Organ Blood Flow*. Bethesda, MD: Am. Physiol. Soc., 1983, sect. 2, vol. III, pt. 2, chapt. 14, p. 453–496.
38. **Sagawa, K., W. L. Maughan, H. Suga, and K. Sunagawa.** *Cardiac Contraction and the Pressure-Volume Relationship*. New York: Oxford Univ. Press, 1988.
39. **Schmidt, R. M., M. Kumada, and K. Sagawa.** Cardiovascular responses to various pulsatile pressures in the carotid sinus. *Am. J. Physiol.* 223: 1–7, 1972.
40. **Sheriff, D. D., D. Kass, C. MacAnespie-Tunin, and K. Sagawa.** Influence of carotid sinus baroreceptor reflex on left ventricular contractility in anesthetized dogs (Abstract). *Circulation* 80, *Suppl.* II: II-553, 1989.
41. **Shigemi, K., M. J. Brunner, and A. A. Shoukas.** α- and β-adrenergic mechanisms in the control of vascular capacitance by the carotid sinus baroreflex system. *Am. J. Physiol.* 267 (*Heart Circ. Physiol.* 36): H201–H210, 1994.
42. **Shoukas, A. A., and M. Brunner.** Epinephrine and the carotid sinus baroreceptor reflex. Influence on capacitive and resistive properties of the total systemic vascular bed of the dog. *Circ. Res.* 47: 249–257, 1980.
43. **Shoukas, A. A., and K. Sagawa.** Control of total systemic vascular capacity by the carotid sinus baroreceptor reflex. *Circ. Res.* 33: 22–32, 1973.
44. **Shroff, S. G., J. S. Janicki, and K. T. Weber.** Evidence and quantitation of left ventricular systolic resistance. *Am. J. Physiol.* 249 (*Heart Circ. Physiol.* 18): H358–H370, 1985.
45. **Suga, H., K. Sagawa, and D. P. Kostiuk.** Controls of ventricular contractility assessed by pressure-volume ratio E_{max}. *Cardiovasc. Res.* 10: 582–592, 1976.
46. **Takeuchi, M., Y. Igarashi, S. Tomimoto, M. Odake, T. Hayashi, T. Tsukamoto, K. Hata, H. Takaoka, and H. Fukuzaki.** Single-beat estimation of the slope of the end-systolic pressure-volume relation in the human left ventricle. *Circulation* 83: 202–212, 1991.
47. **Ursino, M., M. Antonucci, and E. Belardinelli.** The role of active changes in venous capacity by the carotid baroreflex: analysis with a mathematical model. *Am. J. Physiol.* 267 (*Heart Circ. Physiol.* 36): H2531–H2546, 1994.
48. **Wang, W., M. Brändle, and I. H. Zucker.** Influence of vagotomy on the baroreflex sensitivity in anesthetized dogs with experimental heart failure. *Am. J. Physiol.* 265 (*Heart Circ. Physiol.* 34): H1310–H1317, 1993.
49. **Weissler, A. M., W. S. Harris, and C. D. Schoenfeld.** Systolic time intervals in heart failure in man. *Circulation* 37: 149–159, 1968.

Downloaded from http://ajpheart.physiology.org/ by 10.220.33.2 on September 9, 2017